JOURNAL OF MATERIALS SCIENCE 32 (1997) 3595–3600

Density gradient effects on aluminium foam compression behaviour

J. T. BEALS, M. S. THOMPSON
United Technologies Research Centre, East Hartford, CT 06108, USA

The compression properties of an aluminium foam containing a nonuniform density gradient have been examined. Specimens were taken from various locations within the foam slab, and were tested in two directions. Measured foam properties were compared to calculated values using models derived by Ashby and Gibson [1]. The effect of the density gradient on the compression properties and also the energy absorption characteristics of the foam was found to be significant.

1. Introduction

The technology of producing aluminium metal foams has been extensively reviewed [2–5]. These foams are generally fabricated with only 2–20% of the density of the parent metal and yet still retain significant levels of strength and stiffness. The unique properties of metallic foams make them desirable for a wide variety of applications, including filters, thermal barriers, and as a core material for structural sandwich panels. Aluminium foams also have the potential for use in energy absorption [6, 7].

Several companies have recently developed processes capable of manufacturing larger quantities of metal foams using molten metal processing techniques. Alcan International Limited (Canada), has developed a low cost, semi-continuous process for manufacturing large sheets of aluminium foam using gas foaming. In this study, the compressive properties of Alcan's aluminium foam will be discussed with particular emphasis on the effects of the density gradient that develops during fabrication.

2. Material and test procedure

The aluminium foam used in this study was a nearly-closed cell material made by a patented [8] Alcan semi-continuous casting approach that uses aluminium alloys containing ceramic particulates. During the fabrication, gas is injected into the molten alloy containing the particulates, while an impeller is used to rapidly disperse the gas as small bubbles. The particulates of silicon carbide or aluminium oxide, act as a stabilizer by adhering to the gas–liquid interface of the bubble. The liquid foam forms on top of the melt and can be drawn off onto a moving belt to cool and solidify. During solidification, molten metal will drain through the structure due to gravity. The result is a foam sheet with a density gradient through the thickness. The resulting material has a low density section in the middle and a significantly higher density at the bottom. A typical cross-section of an Alcan foam slab used in this study is shown in Fig. 1.

Compression testing was performed on rectangular shaped foam specimens, comprised of a 3003 aluminium alloy containing 10 vol % alumina (Al_2O_3) particulate. The overall slab density of the foam is 0.19 g cm^{-3}, which is approximately 7% of the parent material bulk density. Full thickness specimens (7.6 × 7.6 × 9.0 cm thick) were cut from the slab. The as-cast bottom surface was retained, but a small amount of material (less than 3 mm) was cut from the top of the foam surface to achieve a flat and parallel test specimen. The cutting procedures were selected so as to minimize local cell wall damage. The full thickness specimens were tested in 2 directions, through-thickness and through-width. Additional tests were done on through-thickness specimens that were cut

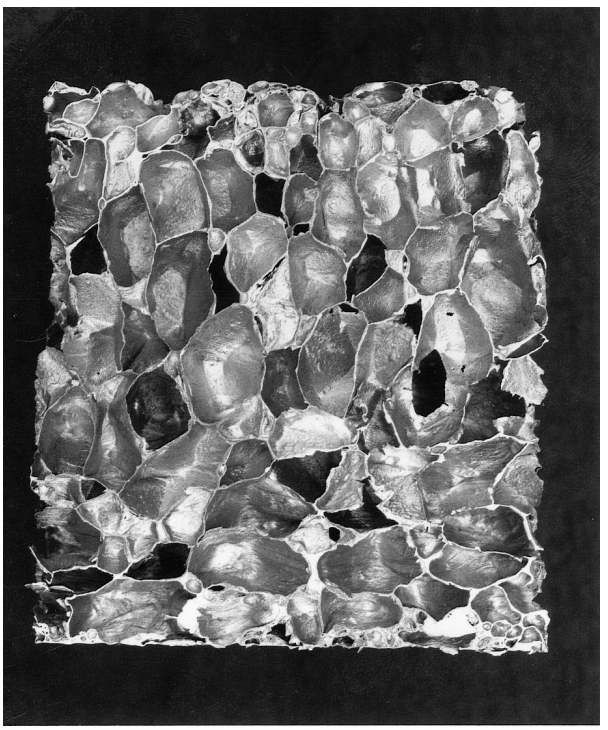

Figure 1 Cross-section of a foam slab showing density gradient.

0022–2461

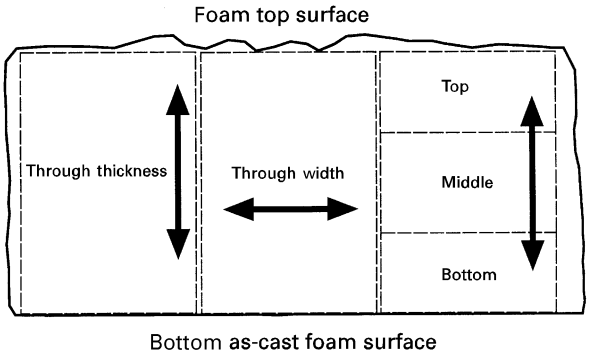

Figure 2 Specimen orientation and position.

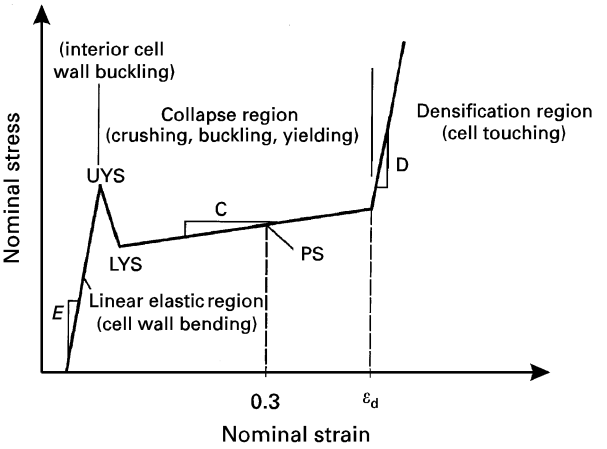

Figure 3 Schematic of foam compression deformation.

into top, middle and bottom sections as is shown in Fig. 2. The figure shows the relative position and orientation for the test specimens within a foam slab with the arrows indicating the loading direction. The dimensions of these specimens were approximately $7.6 \times 7.6 \times 2.5$ cm. Three tests were performed for each direction or position.

The room temperature compression testing was performed at a crosshead rate of $0.02\,\mathrm{cm\,s^{-1}}$ and whenever possible was carried out to a total deformation of 75%. One of the three tests performed for each configuration used extensometry to more accurately measure the foam elastic modulus. Each of the remaining tests used the crosshead displacement to measure the deflection and were video recorded to help observe the deformation process.

3. Results

A schematic depicting features of foam compressive stress–strain behaviour is shown in Fig. 3. Stress is defined as the load per total area of the specimen, including porosity. Likewise, the strain is defined as a nominal value for the foam structure and is not the true strain experienced in the aluminium cell walls. In Fig. 3, three distinct regimes of compressive behaviour can be observed. The first regime is a linear elastic region characterized by an elastic modulus (E). When an upper yield point (UYS) is reached, a load drop can occur. The magnitude of stress reduction to the lower yield point (LYS) appears to be alloy dependent, however, further testing is required to confirm this theory. The second regime that can be seen in the schematic is the "collapse region" that can be characterized by a plateau stress (PS) or if not constant, by a shallow slope (C). The final regime occurs when a critical strain (ε_d) is reached and the cell walls contact. This final regime of densification is characterized by a relatively steep slope (D).

The average measured foam compressive properties are listed in Table 1 for each orientation and position. Three tests were performed for each configuration with good agreement being observed between repeated tests. Representative stress–strain curves are shown in Figs 4 and 5 to demonstrate the effect of specimen orientation and specimen location on the compressive properties. The 3003 alloy foam had significant ductility as displayed by a smooth curve, characteristic

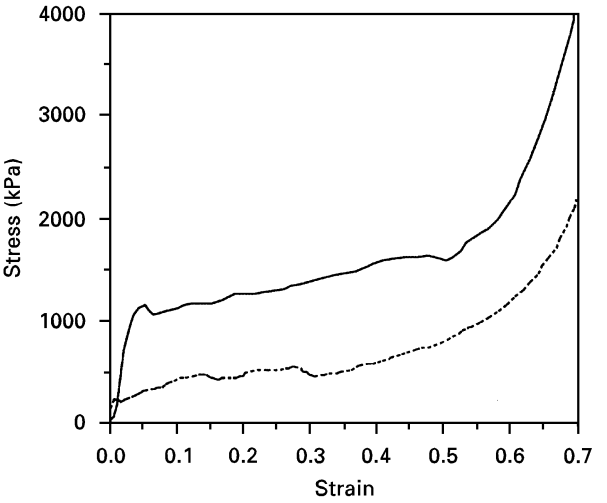

Figure 4 Compressive stress–strain curves for: (—) through width and (⋯ ⋯) through thickness specimen orientations.

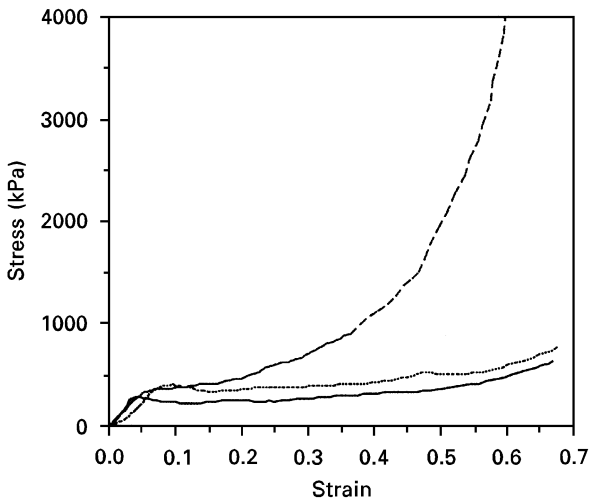

Figure 5 Compressive stress–strain curves for specimen locations of (⋯ ⋯) top, (—) middle and (- - -) bottom.

of plastic foams. Due to the presence of a slight slope in the collapse regime, the plateau stress (PS) is consistently reported in Table I as the stress value for a strain of 0.30 mm. All of the specimens had a densification strain between 0.45–0.70, with most foams

TABLE I Compression test results

Test configuration		Density. ($g\,c^{-1}$)	*UYS*. (kPa)	*C*. (kPa)	*PS*. (kPa)	ε_d	σ_d (kPa)	*D*. (kPa)	*E*. (MPa)
				Full thickness					
Through-thickness	Average	0.20	306	469	407	0.56	538	8 701	204
	Standard deviation	0.01	135	90	62	0.01	104	2 491	–
Through-width	Average	0.20	940	1 297	1 269	0.68	1 787	70 014	217
	Standard deviation	0.01	208	110	173	0.02	152	1 359	–
				Sectioned					
Top	Average	0.12	394	656	407	0.63	676	–	12
	Standard deviation	0	8	222	35	0.04	–	–	–
Middle	Average	0.09	238	352	242	0.63	524	–	39
	Standard deviation	0	35	104	14	0.04	76	–	–
Bottom	Average	0.37	357	1 173	607	0.46	8 280	33 527	16
	Standard deviation	0.04	32	449	90	0.06	152	12 620	–

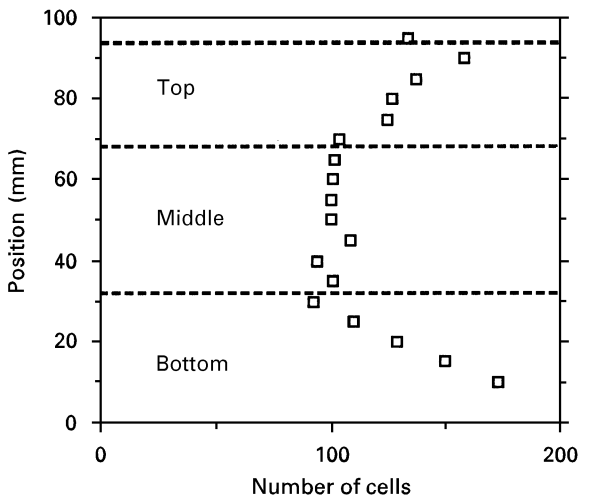

Figure 6 Image analysis data showing variation in the number of cells with position within the thickness direction of foam slab.

exhibiting densification close to 0.60 mm. The *PS* value at a strain of 0.30 was therefore chosen to represent a *median* value. The slopes (*C*) and (*D*) were calculated as best fit curves to the data, with the strain at the onset of densification (ε_d) calculated as the intersection of *C* and *D*. In general, when measuring foam elastic modulus (*E*) it is difficult to obtain predictable or reproducible results.

The average specimen density was determined from the sample weights and physical dimensions for each configuration and are included in Table I. Image analysis of the original slab material was performed to document the extent of the density gradient existing in the top, middle, and bottom sectioned specimens. Multiple sections of foam slab were sectioned in various orientations and prepared so that the position of each cell could be determined. A total of eighteen sections approximately 95×150 mm in cross-sectional area were examined representing over two thousand cells. Fig. 6 summarizes the data with a plot of the number of cells versus cell position in the thickness direction. Assuming that the foam cell wall thickness remains uniform, the number of cells within a cross-sectional area can be correlated to cell size. The change in the number of cells (which is related to cell size) versus position is used here as a good indication of the change in density. Indicated on the figure are the relative positions of the top, middle, and bottom sectioned specimens. Fig. 6 shows that the bottom section contains the largest variation in the number of cells and therefore has the largest density gradient. The top section also shows a significant amount of variation or gradient, while the middle section appears almost uniform in terms of the number of cells.

4. Discussion

The results show a significant variation in the compressive strength properties with specimen orientation. For the full thickness tests, the stress values (*UYS* and *PS*) are significantly higher in the through-width relative to the through-thickness orientation for equivalent density specimens. Gibson and Ashby [1] have derived models that characterize foam behaviour which are further described in the Appendix, with selected relationships being presented in Table II. When using the Gibson and Ashby relationships, which are based on a uniform cell structure, the strength of the foam should be solely dependent on the constitutive parent strength and the relative density of the foam. In this testing, the effect of the density gradient can be clearly seen to affect the failure sequence of the foam. In examining video collected images, it was observed that the initial failure of the foam in the through-thickness direction corresponds to a plane of connected cells in the middle section (lowest density area) of the sample. As deformation continues, cells above or below the initial plane collapse upon it, with the bottom high density area being unaffected until significant deformation has occurred. It is interesting to note that the full section through-thickness *UYS* is very similar to the middle section *UYS* (306 kPa versus 238 kPa). The through-width tested specimens, with the density gradient perpendicular to the loading direction, had failure of cells at several planes. As with the through-thickness testing, failure occurred first within one plane of cells perpendicular to the loading direction. After that plane of cells failed, another plane of cells failed that was not necessarily adjacent to the initial failure location.

TABLE II Ashby and Gibson relationships for predicting foam properties

$$\frac{X_{\text{foam}}}{X_{\text{solid}}} \approx K\left(\frac{\rho_{\text{foam}}}{\rho_{\text{solid}}}\right)^{n}$$

Foam property (X)	K	n
E	1	2
YS	0.3	3/2
Densification strain $= \varepsilon_d = 1 - 1.4\left(\frac{\rho_{\text{foam}}}{\rho_{\text{solid}}}\right)$		

A further understanding of the importance of density and the relationship between changes in density on the deformation event can be seen by comparing the predicted behaviour to the measured results. The relative strength of the foam can be calculated using the Gibson and Ashby equation in Table II. The relative strength for the full thickness density of $0.2\,\text{g}\,\text{cm}^{-3}$ in both directions, as well as the relative strengths for the top, middle, and bottom density foam in the through-thickness direction are calculated and presented in Table III. Normalized by the weakest (middle section) result, a factor of three increase in strength is predicted between the middle section and full thickness results. When normalized in the same way, the UYS or PS data in Table 1 for the through-width direction show an excellent correlation with model results, displaying a similar factor of three increase in the strength. The ratio of the through-thickness to middle section results show poor agreement with the model prediction. This result confirms video recorded observation that strength behaviour in the through-thickness direction is dictated by the performance of the weakest, lowest density plane.

A comparison of the measured foam strength to the predicted behaviour can be made by assuming an approximate value of the parent material yield strength of 138 MPa [9] (Duralcan data for A359/SiC in as-cast condition). The yield strength (UYS) of the foam is calculated for the different densities using the Gibson and Ashby relationship and compared to measured values in Table IV. Excellent agreement can be seen for the top and middle sectioned specimens having little or no density variation, as well as the through-width orientation where compression occurred perpendicular to the direction of significant density gradient. Very poor agreement was seen for the through-thickness orientation and the bottom sectioned specimen where significant density gradients occurred.

TABLE IV Calculated foam UYS values using the Gibson and Ashby relationship

$$UYS = 0.3\text{YS}_{\text{solid}}\left(\frac{\rho_{\text{foam}}}{\rho_{\text{solid}}}\right)^{3/2}$$

Orientation or position	Calculated UYS (kPa)	Measured UYS (kPa)
	Full thickness	
Through-thickness	807	306
Through-width	807	940
	Sectioned	
Top	375	394
Middle	244	238
Bottom	2029	357
($\text{YS}_{\text{solid}} = 138$ MPa)		

The compression behaviour of aluminium foams is important since the material has several other properties that are desirable in an energy absorbing material. One major advantage of aluminium foams over polymer foams is that they offer energy absorption with minimal rebound. Aluminium foams can also be made to withstand higher peak loads and the critical properties can be tailored by changes in the alloy composition, density, cell size and heat treatment.

In its current state the Alcan aluminium foam has a high energy absorption capacity, but only a moderate energy absorption efficiency. The energy absorption capacity of a foam is defined as the maximum energy (area under a compressive load–deflection curve) that can be dissipated by a unit mass of foam. In general, for each application, a maximum allowable peak stress must be defined based on the properties of the impacting body. Excessive stress can contribute to a material with a high energy absorption capacity, but it can also cause damage to the impacting body. The maximum peak stress allowed will vary with use, whether considering body impacts or sensitive packaging. The presence of a UYS followed by a large drop in load can be undesirable in certain applications. In comparing and ranking different energy absorbing materials, it is very useful to calculate the energy absorption efficiency, the ratio of the actual amount of energy absorbed to an ideal total based on the allowable peak stress. Fig. 7(a–c) shows an actual stress–strain curve, an ideal curve, and a schematic on determining the energy absorption efficiency. The schematic shows that for an ideal foam, a plateau

TABLE III Relative strength calculations

Orientation or position	Density ($\text{g}\,\text{cc}^{-1}$)	Relative density	$\sigma_{\text{foam}}/\sigma_{\text{solid}} = 0.3(\rho_{\text{foam}}/\rho_{\text{solid}})^{3/2}$	Ratio to weakest
		Full thickness		
Through-thickness or width	0.20	0.072	5.85×10^{-3}	3.1
		Sectioned		
Top	0.12	0.043	2.72×10^{-3}	1.5
Middle	0.09	0.033	1.77×10^{-3}	1
Bottom	0.37	0.134	0.0147	8.3

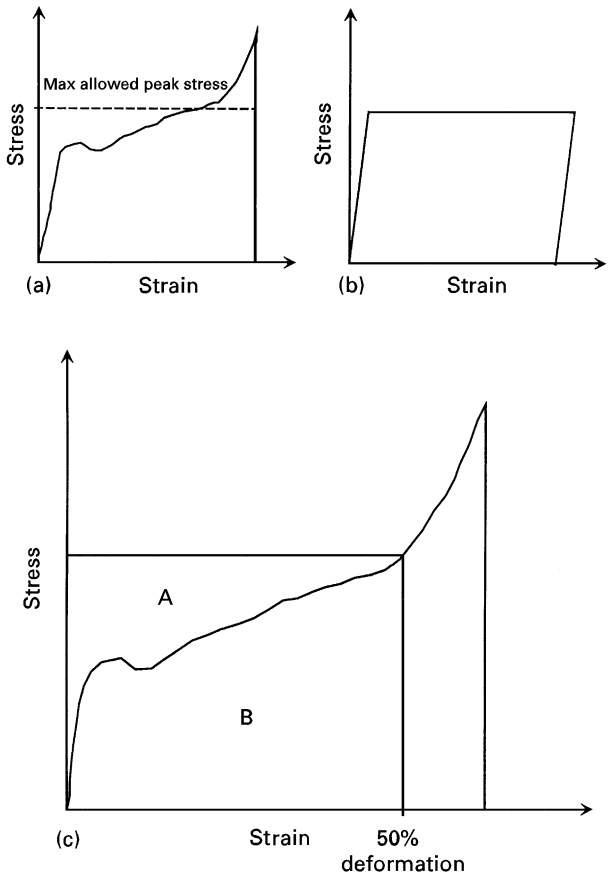

Figure 7 (a) Actual curve, (b) ideal curve and (c) efficiency schematic, note that the energy absorption efficiency is given by $[B/(A + B)] * 100$.

stress equal to the maximum peak stress should be selected. For high efficiency, little or no slope in the collapse region is desired. A large value for densification strain (ε_d) is also desirable, in order to increase the total energy absorbed by the foam.

The density and density gradient can effect the energy absorption efficiency of the foam by influencing both the slope for the collapse region (C) and the densification strain. As described above, to increase the energy absorption efficiency, a low collapse slope and high densification strain are required. The experimental results listed in Table I show significantly higher C values for the large gradient results (through-thickness or bottom section) than for the low gradient results (through-width or middle section). The energy absorption efficiency will therefore be decreased with an increasing density gradient.

The densification strain is directly related to the foam density, with an increasing density creating a decrease in the densification strain. Gibson and Ashby [1] relate ε_d to the relative density or porosity. The densification strain is the point at which a majority of the pore space has been compressed and the cell walls begin to contact. They have also observed that in reality, the cell walls begin to contact each other at a smaller strain value and have identified an empirical relationship for ε_d. This empirical relationship is presented in Table I, and is based mainly on polymer foam testing. Using this relationship, ε_d values between 0.81 and 0.95 are predicted for the density range of aluminium foam tested. The experimental data

TABLE V Energy absorption properties at 50% deformation

Orientation or position	Energy absorption (N·m)	Efficiency (%)
	Full thickness	
Through-thickness	228	79
Through-width	75	85
	Sectioned	
Top	18	71
Middle	13	83
Bottom	20	65

from Table I, while generally following the predicted trend are not well characterized by the empirical Gibson and Ashby relationship. The measured aluminium foam ε_d values are between 0.46 and 0.68 and are thus significantly lower than the predicted values. This indicates that Alcan aluminium foam exhibits densification behaviour at smaller strain values than the polymer foams used to create the model.

The energy absorption properties at 50% deformation and the energy absorption efficiency are listed in Table V for the various foam positions and orientations tested. The specimens with the highest energy absorption efficiency are the full thickness through width and the middle section, that again show the least influence by the density gradient. The lowest efficiency can be seen in the bottom sectioned specimen as a result of the high collapse slope and very low densification strain. The full thickness through thickness foam had the highest energy absorption value because of the high peak stress. However, it does not have a high efficiency primarily due to a low densification strain. The efficiency would be even lower for the through thickness test if the energy absorption was measured at a higher percentage deformation, where there is more influence from the bottom section material.

In practice, the Alcan foam has considerable potential for use as an energy absorbing material. Foam with the bottom section removed shows reasonable efficiency (77%) and when used in a direction independent of the density gradient (through width) an efficiency of 85% is obtained. Higher efficiencies in all directions could be achieved if further process control could result in reduced density gradients. Aluminium foam can be used at peak loads unobtainable in a polymer foam. The use of the material in its current form can also be desirable in applications where complimentary benefits are important. For example, aluminium foam is not sensitive to extreme hot and cold temperatures or high humidity. In a fire, aluminium foam generates no smoke, no flame spread and no toxic gases. Another significant advantage of aluminium foam over a polymer foam is that aluminium foam deforms plastically when impacted and does not spring back, preventing further damage. In energy absorption applications, aluminium foam shows performance characteristics similar to those of an aluminium honeycomb [10] with considerably less anisotropy and with the potential of significantly lower cost.

5. Conclusion

The compressive properties of Alcan aluminium foam were observed to be dependent on the density gradient. Compression failure of the foam was sequential, initiating in the lowest density section and progressing to higher density regions. Relationships derived by Ashby and Gibson [1] to estimate the mechanical properties of cellular materials were found to be useful in approximating the foam compressive strength. The correlation between predicted and experimental results was closest where the influence of the density gradient was minimized. The energy absorption characteristics of the foam are closely tied to the compressive behaviour and strongly dependent on the density gradient. The energy absorption efficiency decreases with an increasing variation in the density.

In its current form, Alcan aluminium foam offers many benefits as an energy absorption material. The foam possesses a high energy absorption capacity and has unique properties that may provide performance advantages over traditional energy absorption materials. Alcan foam samples with a minimal density gradient could offer high efficiency. With a density gradient the material has a lower efficiency, but further process development may result in an optimization of the foam for energy absorption.

Appendix

In general, foam compression properties increase with increasing density, however, they do not do so in a linear manner. Using the mechanisms previously described, Gibson and Ashby [1] have developed models to describe the mechanics of cellular solids. For open celled foams, simple equations are derived that relate the mechanical properties to foam density. The general relationship is a power function:

$$\frac{X_{\text{foam}}}{X_{\text{solid}}} \approx K\left(\frac{\rho_{\text{foam}}}{\rho_{\text{solid}}}\right)^{n} \tag{A1}$$

where X is a property such as the modulus or yield (UYS) strength, with X_{solid} being the parent constituent property. The properties are expressed as a function of relative foam density ($\rho_{\text{foam}}/\rho_{\text{solid}}$) with K an empirically derived constant. Table II lists the values for n and K for a few of the various mechanical properties derived by Gibson and Ashby.

The Gibson and Ashby analysis for closed cell foams is more complex containing contributions due to membrane stretching in the cell faces and from the compression of the encased air within the closed foam cells. The simple open celled foam relationships are used in this study as a general guide to how foam properties can change as a function of density. For this study, Alcan aluminium foam whilst a nearly closed cell, seems to follow the open cell relationships quite well. This type of behaviour has been observed in other closed cell foams made from liquid components [1]. Prior to solidification, surface tension can draw material into the cell edges, leaving only very thin cell faces that easily rupture. The presence of the ceramic particulates in the Alcan foam may also embrittle the thin walls, diminishing the contributions of membrane stretching or compression of the encased air typically seen in closed cell foams.

Gibson and Ashby [1], suggest that the mechanisms of deformation associated with the regimes of deformation in foams parallels that of a honeycomb. The linear elastic range is controlled by cell wall bending. At the upper yield point cells start to buckle and continue to yield through the collapse region. When the cell walls start to touch, densification occurs with rapidly increasing stress.

Acknowledgements

The technical advice of Dr V. Nardone, Dr K. Prewo nd Dr W. Schmidt of UTRC along with Dr U. Koch, S. Hicken and S. Huschka of Daimler Benz was greatly appreciated. Assistance in measuring the foam density gradient was provided by Prof. J. Morral of the University of Connecticut.

References

1. L. J. GIBSON and M. F. ASHBY, in "Cellular solids, structure and properties" (Pergamon Press, Oxford, 1988)
2. M. OTSUKA, N. HOUJO, A. KOJIMA, M. ITOH and E. ISHII, in "Light materials for transportation systems", edited by N. J. Kim (Centre for Advanced Aerospace Materials, Pohang, Korea, 1993) pp. 435–444.
3. G. J. DAVIES and S. ZHEN, *J. Mater. Sci.* **18** (1983) 1899.
4. V. I. SHAPOVALOV, *MRS Bull.* **19** (1994) 24.
5. U. KOCH, M. S. THOMPSON and V. C. NARDONE, in Proceedings of the 4th International Conference on Aluminium Alloys, edited by T. H. Sanders Jr. (The Georgia Institute of Technology, Atlanta, Georgia, 1994) pp. 387–394.
6. P. H. THORNTON and C. L. MAGEE, *Met. Trans. A* **6A** (1975) 1253.
7. L. M. NIEBYLSKI and R. J. FANNING, *SAE Trans.* **81** (1973) 1676.
8. I. JIN, L. D. KENNY and G. SANG, US Patent 4973 358 (1990).
9. Information supplied by Duralcan USA, San Diego, CA (Product Literature)
10. M. BANDAK and T. BITZER, in Proceedings of the 22nd International SAMPE Technical Conference, November 6–8, (SAMPE, Covina, CA, 1990) pp. 1250–1263.

Received 1 May 1995
and accepted 21 October 1996